PHYSICAL REVIEW D **85,** 124062 (2012)

Collisions of charged black holes

Miguel Zilhão,[1,2,3,*] Vitor Cardoso,[4,5] Carlos Herdeiro,[1] Luis Lehner,[2,6] and Ulrich Sperhake[7,8,4]

[1]*Departamento de Física da Universidade de Aveiro and I3N, Campus de Santiago, 3810-183 Aveiro, Portugal*
[2]*Perimeter Institute for Theoretical Physics, Waterloo, Ontario N2L 2Y5, Canada*
[3]*Centro de Física do Porto, Departamento de Física e Astronomia, Faculdade de Ciências da Universidade do Porto, Rua do Campo Alegre, 4169-007 Porto, Portugal*
[4]*Centro Multidisciplinar de Astrofísica—CENTRA, Departamento de Física, Instituto Superior Técnico—IST, Avenida Rovisco Pais 1, 1049-001 Lisboa, Portugal*
[5]*Department of Physics and Astronomy, The University of Mississippi, University, Mississippi 38677-1848, USA*
[6]*Department of Physics, University of Guelph, Guelph, Ontario N1G 2W1, Canada*
[7]*Institut de Ciències de l'Espai (CSIC-IEEC), Facultat de Ciències, Campus UAB, E-08193 Bellaterra, Spain*
[8]*California Institute of Technology, Pasadena, California 91125, USA*

(Received 13 May 2012; published 26 June 2012)

We perform fully nonlinear numerical simulations of charged-black-hole collisions, described by the Einstein-Maxwell equations, and contrast the results against analytic expectations. We focus on head-on collisions of nonspinning black holes, starting from rest and with the same charge-to-mass ratio, Q/M. The addition of charge to black holes introduces a new interesting channel of radiation and dynamics, most of which seem to be captured by Newtonian dynamics and flat-space intuition. The waveforms can be qualitatively described in terms of three stages: (i) an infall phase prior to the formation of a common apparent horizon; (ii) a nonlinear merger phase that corresponds to a peak in gravitational and electromagnetic energy; (iii) the ringdown marked by an oscillatory pattern with exponentially decaying amplitude and characteristic frequencies that are in good agreement with perturbative predictions. We observe that the amount of gravitational-wave energy generated throughout the collision decreases by about 3 orders of magnitude as the charge-to-mass ratio Q/M is increased from 0 to 0.98. We interpret this decrease as a consequence of the smaller accelerations present for larger values of the charge. In contrast, the *ratio* of energy carried by electromagnetic to gravitational radiation increases, reaching about 22% for the maximum Q/M ratio explored, which is in good agreement with analytic predictions.

DOI: 10.1103/PhysRevD.85.124062 PACS numbers: 04.25.D−, 04.25.dg, 04.40.Nr

I. INTRODUCTION

In recent years, numerical relativity (NR) has generated a wealth of information about astrophysical black-hole-binary systems; see [1–3] for the first complete simulations and e.g. [4–10] for a representative list of more recent studies. Results about the dynamics of black holes thus obtained are now actively employed in techniques and searches for gravitational-wave signals in present and future generation gravitational-wave detectors [11–15].

While black-hole binaries interacting with electromagnetic fields and plasmas have been the subject of recent numerical studies (e.g. [5,6]), the dynamics of binary systems of charged, i.e. Reissner-Nordström (RN), black holes remain unexplored territory. Perhaps, this is due to the expectation that astrophysical black holes carry zero or very small charge; in particular, black holes with mass M, charge Q, and angular momentum aM^2 are expected to discharge very quickly if $Q/M \gtrsim 10^{-13}(a/M)^{-1/2}(M/M_\odot)^{1/2}$ [16,17].

In spite of this expectation, however, there is a good deal of motivation for detailed investigations of the dynamics of charged black holes.

We first note that RN black holes possess a unique property amongst the black-hole solutions of Einstein-Maxwell theory in four dimensions. They possess an extremal limit, which can be used to construct a static, regular (on and outside the event horizon) multi-black-hole configuration [18] (described by the Majumdar-Papapetrou solution [19,20]). This configuration can be interpreted as an exact cancellation, at each point, of the attractive (gravitational) and repulsive (electromagnetic) interactions—a *no force condition*. This condition is typically (but not always) associated with supersymmetric configurations, and indeed the extremal RN solution is the only black-hole solution in four-dimensional Einstein-Maxwell theory that admits Killing spinors, when the theory is regarded as the bosonic sector of $\mathcal{N} = 2$ supergravity [21,22]. A natural question concerning the modeling of RN black holes in NR is how close can we get to extremality and hence consider the dynamics of these very special black holes. The ability to model such systems could provide interesting applications. For instance it is possible to study analytically the dynamics of a perturbed Majumdar-Papapetrou solution in the so-called moduli space approximation [23,24]. It would be interesting to compare this analytic approximation method with a fully nonlinear NR simulation.

*Electronic address: mzilhao@fc.up.pt

Motivation for the numerical modeling of charged black holes also arises in the context of high-energy collisions. It is expected that trans-Planckian particle collisions form black holes; moreover, well above the fundamental Planck scale such processes should be well described by general relativity and other interactions should become negligible [25], an idea poetically stated as *matter does not matter* for ultra high-energy collisions [26]. But is this expectation really correct? Calculations of shock wave collisions suggest that even though other interactions—say charge—may become irrelevant in the ultrarelativistic limit, the properties of the final black hole (and of the associated emission of gravitational radiation) do depend on the amount of charge carried by the colliding particles [27,28]. This issue can be clarified by the simulation of high-energy collisions of charged black holes in the framework of NR and the subsequent comparison of the results to those obtained for electrically neutral systems. Recent works in this direction include [29–35] for binary black holes and [26] for boson stars. These, together with related incipient efforts to study gravity in higher-dimensional spacetimes [36–40], illustrate recent applications of numerical simulations to shed light on problems beyond astrophysical settings.

In the context of astrophysics, charged black holes may be of interest in realistic systems. First, a rotating black hole in an external magnetic field will accrete charged particles up to a given value, $Q = 2B_0J$ [41]. Thus it is conceivable that astrophysical black holes could have some (albeit rather small) amount of electrical charge. Then it is of interest to understand the role of this charge in the Blandford-Znajek mechanism [17], which has been suggested for extracting spin energy from the hole, or in a related mechanism capable of extracting energy from a moving black hole [6,42] to power outflows from accretion disk-fed black holes. NR simulations of charged black holes interacting with matter and surrounding plasma will enable us to study such effects.

Finally we note a variety of conceptual aspects that merit a more detailed investigation of charged black-hole systems. In head-on collisions with small velocity, the intuition borrowed from Larmor's formula in Minkowski space suggests a steady growth of the emitted power with the acceleration. However, it is by now well established that for uncharged black holes the gravitational radiation strongly peaks near the time of formation of a common apparent horizon. Does the electromagnetic radiation emission follow a similar pattern? And what is the relative fraction of electromagnetic to gravitational-wave emissions? Moreover, a non-head-on collision of charged nonspinning black holes will allow us to study, as the end state, a (perturbed) Kerr-Newman geometry, which would be extremely interesting: linearized perturbations around Kerr-Newman black holes do not decouple [43,44], and so far close to nothing is known about their properties. Among others, the stability of the Kerr-Newman metric is an outstanding open issue. Furthermore, it has been observed that the inspiral phase of an orbiting black-hole-binary system can be well understood via post-Newtonian methods [45] (see also e.g. [46,47]). The additional radiative channel opened by the presence of electric charge provides additional scope to probe this observation.

With the above motivation in mind we here initiate the numerical study of nonlinear dynamics of binary systems of RN black holes, building on previous numerical evolutions of the Einstein-Maxwell system [5,48–50]. For reasons of simplicity, we focus in this study on binary systems for which initial data can be constructed by purely analytic means [51,52]: head-on collisions, starting from rest, of nonspinning black holes with equal charge-to-mass ratio. This implies, in particular, that the black holes carry a charge of the same *sign* so that the electromagnetic force will always be repulsive. We will extract both gravitational and electromagnetic radiation and monitor their behavior as the charge-to-mass-ratio parameter of the system is varied.

For this purpose, we present in Sec. II the evolution equations and the initial data used. In Sec. III the method for extraction of gravitational and electromagnetic radiation is discussed. In Sec. IV we summarize our analytic calculations, and in Sec. V we compare their predictions with the numerical results. Throughout this work greek "spacetime indices" run from 0 to 3 and latin "spatial" indices from 1 to 3.

II. EVOLUTION EQUATIONS

In this paper we adopt the approach outlined in [49,53] to evolve the electrovacuum Einstein-Maxwell equations, which incorporates suitably added additional fields to ensure the evolution will preserve the constraints. This amounts to considering an enlarged system of the form

$$\begin{aligned} R_{\mu\nu} - \frac{R}{2} g_{\mu\nu} &= 8\pi T_{\mu\nu}, \\ \nabla_\mu (F^{\mu\nu} + g^{\mu\nu}\Psi) &= -\kappa n^\nu \Psi, \\ \nabla_\mu (\star F^{\mu\nu} + g^{\mu\nu}\Phi) &= -\kappa n^\nu \Phi, \end{aligned} \tag{2.1}$$

where $\star F^{\mu\nu}$ denotes the Hodge dual of the Maxwell-Faraday tensor $F^{\mu\nu}$, κ is a constant, and n^μ is the four-velocity of the Eulerian observer. We recover the standard Einstein-Maxwell system of equations when $\Psi = 0 = \Phi$. With the scalar field Ψ and pseudoscalar Φ introduced in this way, the natural evolution of this system drives Ψ and Φ to zero (for positive κ), thus ensuring the magnetic and electric constraints are controlled [48,53]. The electromagnetic stress-energy tensor takes the usual form

$$T_{\mu\nu} = \frac{1}{4\pi}\left[F_\mu{}^\lambda F_{\nu\lambda} - \frac{1}{4} g_{\mu\nu} F^{\lambda\sigma} F_{\lambda\sigma} \right]. \tag{2.2}$$

A. 3 + 1 decomposition

We employ a Cauchy approach so we introduce a 3 + 1 decomposition of all dynamical quantities. Concretely, we introduce the 3-metric

$$\gamma_{\mu\nu} = g_{\mu\nu} + n_\mu n_\nu, \tag{2.3}$$

and decompose the Maxwell-Faraday tensor into the more familiar electric and magnetic fields measured by the Eulerian observer moving with four-velocity n^μ

$$\begin{aligned} F_{\mu\nu} &= n_\mu E_\nu - n_\nu E_\mu + \epsilon_{\mu\nu\alpha\beta} B^\alpha n^\beta, \\ \star F_{\mu\nu} &= n_\mu B_\nu - n_\nu B_\mu - \epsilon_{\mu\nu\alpha\beta} E^\alpha n^\beta, \end{aligned} \tag{2.4}$$

where we use the convention $\epsilon_{1230} = \sqrt{-g}$, $\epsilon_{\alpha\beta\gamma} = \epsilon_{\alpha\beta\gamma\delta} n^\delta$, $\epsilon_{123} = \sqrt{\gamma}$.

Writing the evolution equations in the Baumgarte, Shapiro, Shibata, and Nakamura (BSSN) form (see, e.g., [54,55] for details), we have, for the "gravitational" part,

$$\tilde{\gamma}_{ij} = \chi \gamma_{ij}, \qquad \chi = \gamma^{-1/3}, \qquad \tilde{A}_{ij} \equiv \chi\left(K_{ij} - \frac{\gamma_{ij}}{3} K\right), \tag{2.5}$$

$$\begin{aligned} (\partial_t - \mathcal{L}_\beta)\tilde{\gamma}_{ij} &= -2\alpha \tilde{A}_{ij}, \\ (\partial_t - \mathcal{L}_\beta)\chi &= \frac{2}{3}\alpha \chi K, \\ (\partial_t - \mathcal{L}_\beta)K &= [\ldots] + 4\pi\alpha(\rho + S), \\ (\partial_t - \mathcal{L}_\beta)\tilde{A}_{ij} &= [\ldots] - 8\pi\alpha\left(\chi S_{ij} - \frac{S}{3}\tilde{\gamma}_{ij}\right), \\ (\partial_t - \mathcal{L}_\beta)\tilde{\Gamma}^i &= [\ldots] - 16\pi\alpha\chi^{-1} j^i, \quad \tilde{\Gamma}^i = \tilde{\gamma}^{jk}\tilde{\Gamma}^i_{jk}, \end{aligned} \tag{2.6}$$

where [...] denotes the standard right-hand side of the BSSN equations in the absence of source terms. For the case of the electromagnetic energy-momentum tensor of Eqs. (2.2) and (2.1), the source terms are given by

$$\begin{aligned} \rho &\equiv T^{\mu\nu} n_\mu n_\nu = \frac{1}{8\pi}(E^2 + B^2), \\ j_i &\equiv -\gamma_{i\mu} T^{\mu\nu} n_\nu = \frac{1}{4\pi}\epsilon_{ijk} E^j B^k, \\ S_{ij} &\equiv \gamma_i^\mu \gamma_j^\nu T_{\mu\nu} = \frac{1}{4\pi}\left[-E_i E_j - B_i B_j + \frac{1}{2}\gamma_{ij}(E^2 + B^2)\right], \end{aligned} \tag{2.7}$$

and $S \equiv \gamma^{ij} S_{ij}$. The evolution of the electromagnetic fields is determined by Eq. (2.1) whose 3 + 1 decomposition becomes [50]

$$\begin{aligned} (\partial_t - \mathcal{L}_\beta)E^i &= \alpha K E^i + \epsilon^{ijk}\chi^{-1}[\tilde{\gamma}_{kl} B^l \partial_j \alpha + \alpha(B^l \partial_j \tilde{\gamma}_{kl} + \tilde{\gamma}_{kl}\partial_j B^l - \chi^{-1}\tilde{\gamma}_{kl} B^l \partial_j \chi)] - \alpha\chi\tilde{\gamma}^{ij}\partial_j \Psi, \\ (\partial_t - \mathcal{L}_\beta)B^i &= \alpha K B^i - \epsilon^{ijk}\chi^{-1}[\tilde{\gamma}_{kl} E^l \partial_j \alpha + \alpha(E^l \partial_j \tilde{\gamma}_{kl} + \tilde{\gamma}_{kl}\partial_j E^l - \chi^{-1}\tilde{\gamma}_{kl} E^l \partial_j \chi)] - \alpha\chi\tilde{\gamma}^{ij}\partial_j \Phi, \\ (\partial_t - \mathcal{L}_\beta)\Psi &= -\alpha\nabla_i E^i - \alpha\kappa\Psi, \qquad (\partial_t - \mathcal{L}_\beta)\Phi = -\alpha\nabla_i B^i - \alpha\kappa\Phi. \end{aligned} \tag{2.8}$$

Here, $\mathcal{L}_\beta$ denotes the Lie derivative along the shift vector β^i. The Hamiltonian and momentum constraint are

$$\begin{aligned} \mathcal{H} &\equiv {}^3R + K^2 - K^{ij}K_{ij} - 16\pi\rho = 0, \\ \mathcal{M}_i &\equiv D_j A_i{}^j - \frac{3}{2}A_i{}^j\chi^{-1}\partial_j\chi - \frac{2}{3}\partial_i K - 8\pi j_i = 0, \end{aligned} \tag{2.9}$$

where D_i is the covariant derivative associated with the three-metric γ_{ij}.

B. Initial data

As already mentioned in the Introduction, we focus here on black-hole binaries with equal charge and mass colliding from rest. For these configurations, it is possible to construct initial data using the Brill-Lindquist construction [51] (see also [52]). The main ingredients of this procedure are as follows.

For a vanishing shift β^i, time symmetry implies $K_{ij} = 0$. Combined with the condition of an initially vanishing magnetic field, the magnetic constraint $D_i B^i = 0$ and momentum constraint are automatically satisfied. By further assuming the spatial metric to be conformally flat

$$\gamma_{ij} dx^i dx^j = \psi^4(dx^2 + dy^2 + dz^2), \tag{2.10}$$

the Hamiltonian constraint reduces to

$$\triangle \psi = -\tfrac{1}{4}E^2\psi^5, \tag{2.11}$$

where $\triangle$ is the flat-space Laplace operator. The electric constraint, Gauss's law, has the usual form

$$D_i E^i = 0. \tag{2.12}$$

Quite remarkably, for systems of black holes with equal charge-to-mass ratio, these equations have known analytical solutions [52]. For the special case of two black holes momentarily at rest with "bare masses" m_1, m_2 and "bare charges" q_1, $q_2 = q_1 m_2/m_1$, this analytic solution is given by

$$\psi^2 = \left(1 + \frac{m_1}{2|\vec{x}-\vec{x}_1|} + \frac{m_2}{2|\vec{x}-\vec{x}_2|}\right)^2 - \frac{1}{4}\left(\frac{q_1}{|\vec{x}-\vec{x}_1|} + \frac{q_2}{|\vec{x}-\vec{x}_2|}\right)^2, \qquad (2.13)$$

$$E^i = \psi^{-6}\left(q_1 \frac{(\vec{x}-\vec{x}_1)^i}{|\vec{x}-\vec{x}_1|^3} + q_2 \frac{(\vec{x}-\vec{x}_2)^i}{|\vec{x}-\vec{x}_2|^3}\right),$$

where $\vec{x}_i$ is the coordinate location of the ith "puncture."[1]

The initial data are thus completely specified in terms of the independent mass and charge parameters m_1, m_2, and q_1 and the initial coordinate separation d of the holes. These uniquely determine the remaining charge parameter q_2 via the condition of the equal charge-to-mass ratio. In this study we always choose $m_1 = m_2$ and, without loss of generality, position the two holes symmetrically around the origin such that $z_1 = d/2 = -z_2$. The resulting initial three-metric γ_{ij} follows from Eqs. (2.10) and (2.13) while the extrinsic curvature K_{ij} and magnetic field B^i vanish on the initial slice.

Finally, the time evolution of the fields is determined by Eqs. (2.5) and (2.8). We use the same gauge conditions and outer boundary conditions for the BSSN variables as used in vacuum simulations [56]. As outer boundary condition for the electric and magnetic fields we have imposed a falloff as $1/r^2$—from (2.13). For the additional scalar fields a satisfactory behavior is observed by imposing a falloff as $1/r^3$ (which is the expected falloff rate from dimensional grounds).

III. WAVE EXTRACTION

For a given set of initial parameters $m_1 = m_2$, $q_1 = q_2$, and d, the time evolution provides us with the spatial metric γ_{ij}, the extrinsic curvature K_{ij}, as well as the electric and magnetic fields E^i, B^i as functions of time. These fields enable us to extract the gravitational and electromagnetic radiation as follows.

For the gravitational-wave signal we calculate the Newman-Penrose scalar Ψ_4 defined as

$$\Psi_4 \equiv C_{\alpha\beta\gamma\delta} k^\alpha \bar{m}^\beta k^\gamma \bar{m}^\delta, \qquad (3.1)$$

where $C_{\alpha\beta\gamma\delta}$ is the Weyl tensor and k, $\bar{m}$ are part of a null tetrad l, k, m, $\bar{m}$ satisfying $-l\cdot k = 1 = m\cdot\bar{m}$; all other inner products vanish. In practice l, k, and m are constructed from an orthonormal triad u, v, w orthogonal to the unit timelike vector n^μ:

$$l^\alpha = \frac{1}{\sqrt{2}}(n^\alpha + u^\alpha), \qquad k^\alpha = \frac{1}{\sqrt{2}}(n^\alpha - u^\alpha),$$
$$m^\alpha = \frac{1}{\sqrt{2}}(v^\alpha + iw^\alpha). \qquad (3.2)$$

[1]We note that this foliation, in isotropic coordinates, covers only the outside of the external horizon.

We refer the interested reader to [57] for more details about the numerical implementation and [58] for a review of the formalism; here we merely note that asymptotically the triad vectors u, v, and w behave as the unit radial, polar, and azimuthal vectors $\hat{r}$, $\hat{\theta}$, and $\hat{\phi}$.

Similarly, we extract the electromagnetic wave signal in the form of the scalar functions, Φ_1 and Φ_2 [59], defined as

$$\Phi_1 \equiv \tfrac{1}{2}F_{\mu\nu}(l^\mu k^\nu + \bar{m}^\mu m^\nu), \qquad (3.3)$$

$$\Phi_2 \equiv F_{\mu\nu}\bar{m}^\mu k^\nu. \qquad (3.4)$$

For outgoing waves at infinity, these quantities behave as

$$\Phi_1 \sim \tfrac{1}{2}(E_{\hat{r}} + iB_{\hat{r}}), \qquad \Phi_2 \sim E_{\hat{\theta}} - iE_{\hat{\phi}}. \qquad (3.5)$$

At a given extraction radius $R_{\rm ex}$, we perform a multipolar decomposition by projecting Ψ_4, Φ_1, and Φ_2 onto spherical harmonics of spin weights $s = -2$, 0, and -1, respectively:

$$\Psi_4(t,\theta,\phi) = \sum_{l,m} \psi^{lm}(t) Y^{-2}_{lm}(\theta,\phi), \qquad (3.6)$$

$$\Phi_1(t,\theta,\phi) = \sum_{l,m} \phi_1^{lm}(t) Y^{0}_{lm}(\theta,\phi), \qquad (3.7)$$

$$\Phi_2(t,\theta,\phi) = \sum_{l,m} \phi_2^{lm}(t) Y^{-1}_{lm}(\theta,\phi). \qquad (3.8)$$

In terms of these multipoles, the radiated flux and energy is given by the expressions [59]

$$F_{\rm GW} = \frac{dE_{\rm GW}}{dt} = \lim_{r\to\infty}\frac{r^2}{16\pi}\sum_{l,m}\left|\int_{-\infty}^{t} dt' \psi^{lm}(t')\right|^2, \qquad (3.9)$$

$$F_{\rm EM} = \frac{dE_{\rm EM}}{dt} = \lim_{r\to\infty}\frac{r^2}{4\pi}\sum_{l,m}|\phi_2^{lm}(t)|^2. \qquad (3.10)$$

As is well known from simulations of uncharged black-hole binaries, initial data obtained from the Brill-Lindquist construction contain "spurious" radiation, which is an artifact of the conformal-flatness assumption. In calculating properties of the radiation, we account for this effect by starting the integration of the radiated flux in Eqs. (3.9) and (3.10) at some finite time Δt after the start of the simulation, thus allowing the spurious pulse to first radiate off the computational domain. In practice, we obtain satisfactory results by choosing $\Delta t = R_{\rm ex} + 50M$. Because the physical radiation is very weak for both the gravitational and electromagnetic channel in this early infall stage, the error incurred by this truncation is negligible compared with the uncertainties due to discretization; cf. Sec. V D.

IV. ANALYTIC PREDICTIONS

Before discussing in detail the results of our numerical simulations, it is instructive to discuss the behavior of the

binary system as expected from an analytic approximation. Such an analysis not only serves an intuitive understanding of the binary's dynamics, but also provides predictions to compare with the numerical results presented below.

For this purpose we consider the electrodynamics of a system of two equal point charges in a Minkowski background spacetime. As in the black-hole case, we denote by $q_1 = q_2 \equiv Q/2$ and $m_1 = m_2 \equiv M/2$ the electric charge and mass of the particles that are initially at rest at position $z = \pm d/2$.

It turns out to be useful to first consider point charges in Minkowski spacetime in the static limit. The expected behavior of the radial component of the resulting electric field is given by [60]

$$E_{\hat{r}} = 4\pi \sum_{l,m} \frac{l+1}{2l+1} q_{lm} \frac{Y_{lm}(\theta, \varphi)}{r^{l+2}}, \tag{4.1}$$

which for a system of two charges of equal magnitude at $z = \pm d/2$ becomes

$$E_{\hat{r}} \simeq \sqrt{4\pi} Q \frac{Y_{00}}{r^2} + \sqrt{\frac{9\pi}{20}} Q d^2 \frac{Y_{20}}{r^4}. \tag{4.2}$$

The dipole vanishes in this case due to the reflection symmetry across $z = 0$. This symmetry is naturally preserved during the time evolution of the two-charge system. Furthermore, the total electric charge Q is conserved so that the leading-order behavior of the electromagnetic radiation is given by variation of the electric quadrupole, just as for the gravitational radiation. Notice that in principle other radiative contributions can arise from the accelerated motion of the charged black holes. From experience with gravitational radiation generated in the collision of electrically neutral black-hole binaries, however, we expect this "Bremsstrahlung" to be small in comparison with the merger signal and hence ignore its contributions in this simple approximation. The good agreement with the numerical results presented in the next section bears out the validity of this *quadrupole approximation*. In consequence, it appears legitimate to regard the "strength" of the collision and the excitation of the black-hole ringdown to be purely kinematic effects.

An estimate for the monopole and quadrupole amplitudes in the limit of two static point charges is then obtained from inserting the radial component of the electric field (4.2) into the expression (3.5) for Φ_1 and its multipolar decomposition (3.7)

$$r^2 \phi_1^{00} = \sqrt{\pi} Q \approx 1.77 Q, \tag{4.3}$$

$$r^4 \phi_1^{20} = \sqrt{\frac{9\pi}{80}} Q d^2 \approx 0.59 Q d^2. \tag{4.4}$$

The expectation is that these expressions provide a good approximation for the wave signal during the early infall stage when the black holes are moving with small velocities. Equation (4.3) should also provide a good approximation for ϕ_1^{00} after the merger and ringdown, whereas the quadrupole ϕ_1^{20} should eventually approach zero as a single merged hole corresponds to the case $d = 0$ in Eq. (4.4).

To obtain analytic estimates for the collision time and the emitted radiation, we need to describe the dynamic behavior of the two point charges. Our starting point for this discussion is the combined gravitational and electromagnetic potential energy for two charges $i = 1, 2$ in Minkowski spacetime with mass and charge m_i, q_i at distance r from each other

$$V = -\frac{G m_1 m_2}{r} + \frac{1}{4\pi\epsilon_0} \frac{q_1 q_2}{r}. \tag{4.5}$$

For the case of two charges with equal mass and charge $m_i = M/2$, $q_i = Q/2$ and starting from rest at $z_0 = \pm d/2$, conservation of energy implies

$$M\dot{z}^2 - \frac{M^2 \mathcal{B}}{4z} = -\frac{M^2 \mathcal{B}}{2d}, \tag{4.6}$$

where we have used units with $G = 4\pi\epsilon_0 = 1$ and

$$\mathcal{B} \equiv 1 - Q^2/M^2. \tag{4.7}$$

The resulting equation of motion for $z(t)$ is obtained by differentiating Eq. (4.6), which results in

$$M\ddot{z} = -\frac{M^2}{8z^2} + \frac{Q^2}{8z^2} = -M^2 \frac{\mathcal{B}}{8z^2}. \tag{4.8}$$

An estimate for the time for collision follows from integrating Eq. (4.6) over $z \in [d/2, 0]$

$$\left(\frac{t_{\text{collision}}}{M}\right)^2 = \frac{\pi^2 d^3}{2^3 M^3 \mathcal{B}}. \tag{4.9}$$

From the dynamic evolution of the system we can derive an approximate prediction for the electromagnetic radiation by evaluating the (traceless) electric quadrupole tensor $Q_{ij} = \int d^3\vec{x}\rho(\vec{x})(3x_i x_j - r^2\delta_{ij})$ [60]. In terms of this quadrupole tensor, the total power radiated is given by [60]

$$F_{\text{EM}} = \sum_{ij} \frac{1}{4\pi\epsilon_0} \frac{1}{360 c^5} \dddot{Q}_{ij}. \tag{4.10}$$

For clarity we have reinstated the factors $4\pi\epsilon_0$ and c^5 here. Using

$$\frac{d^3}{dt^3}(z^2) = 6\dot{z}\,\ddot{z} + 2z\dddot{z}, \tag{4.11}$$

and the equations of motion (4.6) and (4.8) we find

$$F_{\text{EM}} = \frac{\mathcal{B}^3 M^3 Q^2 (1/z - 2/d)}{1920 z^4}. \tag{4.12}$$

Using $\int dt(\ldots) = \int dz/\dot{z}(\ldots)$, we can evaluate the time integral up to some cutoff separation, say $z_{\min} = \alpha_b b$, where b is the horizon radius of the initial black hole, $b = M(1 + \sqrt{\mathcal{B}})/2$, and $\alpha_b = \mathcal{O}(1)$ is a constant. This gives

$$\frac{E_{\rm rad}^{\rm EM}}{M} = \mathcal{B}^{5/2} M^{3/2} Q^2 \frac{(d-2\alpha_b b)^{3/2}(15d^2+24d\alpha_b b+32\alpha_b^2 b^2)}{50\,400(d\alpha_b b)^{7/2}}. \tag{4.13}$$

Emission of gravitational radiation follows from the quadrupole formula, which is a numerical factor 4 times larger, and where the charge is be replaced by the mass,

$$\frac{E_{\rm rad}^{\rm GW}}{M} = \mathcal{B}^{5/2} M^{7/2} \frac{(d-2\alpha_b b)^{3/2}(15d^2+24d\alpha_b b+32\alpha_b^2 b^2)}{12\,600(d\alpha_b b)^{7/2}}. \tag{4.14}$$

For $Q = 0$, $\alpha_b = 1$, and $d = \infty$ we thus obtain

$$\frac{E_{\rm rad}^{\rm GW}}{M} = \frac{1}{840} \sim 0.0012, \tag{4.15}$$

in agreement to within a factor of 2 with numerical simulations (see [33] and Table I below; the agreement could be improved by assuming $\alpha_b \sim 1.3$). As a general result of this analysis we find in this approximation

$$\frac{E_{\rm rad}^{\rm EM}}{E_{\rm rad}^{\rm GW}} = \frac{Q^2}{4M^2}. \tag{4.16}$$

For nonextremal holes $Q < M$, our analytic considerations therefore predict that the energy emitted in electromagnetic radiation is at most 25% of the energy lost in gravitational radiation. As we shall see below, this turns out to be a remarkably good prediction for the results obtained from fully numerical simulations.

V. NUMERICAL RESULTS

The numerical integration of the Einstein-Maxwell equations (2.6) and (2.8) has been performed using fourth-order spatial discretization with the LEAN code, originally presented in [57] for vacuum spacetimes. LEAN is based on the CACTUS Computational toolkit [61] and the CARPET mesh refinement package [62,63] and uses AHFINDERDIRECT for tracking apparent horizons [64,65]. For further details of the numerical methods see Ref. [57].

The initial parameters as well as the grid setup and the radiated gravitational and electromagnetic wave energy for our set of binary configurations is listed in Table I. All binaries start from rest with a coordinate distance $d/M \simeq 8$ or $d/M \simeq 16$ while the charge-to-mass ratio has been varied from $Q/M = 0$ to $Q/M = 0.98$. Note that identical coordinate separations of the punctures for different values

TABLE I. Grid structure in the notation of Sec. II E of [57], coordinate distance d/M, proper horizon-to-horizon distance L/M, charge Q/M, and gravitational ($E_{\rm rad}^{\rm GW}$) and electromagnetic ($E_{\rm rad}^{\rm EM}$) radiated energy for our set of simulations. The radiated energy has been computed using only the $l = 2$, $m = 0$ mode; the energy contained higher-order multipoles such as $l = 4$, $m = 0$ is negligible for all configurations.

Run	Grid	d/M	L/M	Q/M	$E_{\rm rad}^{\rm GW}$	$E_{\rm rad}^{\rm EM}$
d08q00	$\{(256, 128, 64, 32, 16, 8) \times (2, 1, 0.5), 1/80\}$	8.002	11.56	0	5.1×10^{-4}	n.a.
d08q03	$\{(256, 128, 64, 32, 16, 8) \times (2, 1, 0.5), 1/80\}$	8.002	11.60	0.3	4.5×10^{-4}	1.3×10^{-5}
d08q04	$\{(256, 128, 64, 32, 16, 8) \times (2, 1, 0.5), 1/80\}$	8.002	11.65	0.4	4.0×10^{-4}	2.1×10^{-5}
d08q05c	$\{(256, 128, 64, 32, 16, 8) \times (2, 1, 0.5), 1/64\}$	8.002	11.67	0.5	3.3×10^{-4}	2.7×10^{-5}
d08q05m	$\{(256, 128, 64, 32, 16, 8) \times (2, 1, 0.5), 1/80\}$	8.002	11.70	0.5	3.4×10^{-4}	2.7×10^{-5}
d08q05f	$\{(256, 128, 64, 32, 16, 8) \times (2, 1, 0.5), 1/96\}$	8.002	11.67	0.5	3.4×10^{-4}	2.7×10^{-5}
d08q055	$\{(256, 128, 64, 32, 16, 8) \times (2, 1, 0.5), 1/80\}$	8.002	11.70	0.55	3.0×10^{-4}	2.89×10^{-5}
d08q06	$\{(256, 128, 64, 32, 16, 8) \times (2, 1, 0.5), 1/80\}$	8.002	11.75	0.6	2.6×10^{-4}	2.97×10^{-5}
d08q07	$\{(256, 128, 64, 32, 16, 8) \times (2, 1, 0.5), 1/80\}$	8.002	11.87	0.7	1.8×10^{-4}	2.7×10^{-5}
d08q08	$\{(256, 128, 64, 32, 16, 8) \times (2, 1, 0.5), 1/80\}$	8.002	12.0	0.8	9.8×10^{-5}	1.8×10^{-5}
d08q09	$\{(256, 128, 64, 32, 16, 8) \times (2, 1, 0.5), 1/80\}$	8.002	12.3	0.9	2.6×10^{-5}	5.5×10^{-6}
d08q098cc	$\{(256, 128, 64, 32, 16, 8) \times (2, 1, 0.5), 1/64\}$	8.002	12.3	0.98	7.0×10^{-7}	2.1×10^{-7}
d08q098c	$\{(256, 128, 64, 32, 16, 8) \times (2, 1, 0.5), 1/80\}$	8.002	13.1	0.98	4.3×10^{-7}	1.4×10^{-7}
d08q098m	$\{(256, 128, 64, 32, 16, 8) \times (2, 1, 0.5), 1/96\}$	8.002	13.1	0.98	3.4×10^{-7}	1.0×10^{-7}
d08q098f	$\{(256, 128, 64, 32, 16, 8) \times (2, 1, 0.5), 1/112\}$	8.002	13.0	0.98	4.0×10^{-7}	9.5×10^{-8}
d08q098ff	$\{(256, 128, 64, 32, 16, 8) \times (2, 1, 0.5), 1/128\}$	8.002	13.0	0.98	4.05×10^{-7}	8.75×10^{-8}
d08q098fff	$\{(256, 128, 64, 32, 16, 8) \times (2, 1, 0.5), 1/136\}$	8.002	13.1	0.98	3.73×10^{-7}	8.41×10^{-8}
d16q00	$\{(256, 128, 64, 32, 16) \times (4, 2, 1, 0.5), 1/64\}$	16.002	20.2	0	5.5×10^{-4}	n.a.
d16q05	$\{(256, 128, 64, 32, 16) \times (4, 2, 1, 0.5), 1/64\}$	16.002	20.3	0.5	3.6×10^{-4}	2.9×10^{-5}
d16q08	$\{(256, 128, 64, 32, 16) \times (4, 2, 1, 0.5), 1/80\}$	16.002	20.7	0.8	1.05×10^{-4}	1.9×10^{-5}
d16q09	$\{(256, 128, 64, 32, 16) \times (4, 2, 1, 0.5), 1/80\}$	16.002	21.0	0.9	2.7×10^{-5}	5.9×10^{-6}

of the charge Q/M correspond to different horizon-to-horizon proper distances. This difference is expected, and in fact analysis of the RN solution predicts a divergence of the proper distance in the limit $Q/M \to 1$.

A. Code tests

Before discussing the obtained results in more detail, we present two tests to validate the performance of our numerical implementation of the evolution equations: (i) single black-hole evolutions in *geodesic slicing*, which is known to result in numerical instabilities after relatively short times but facilitates direct comparison with a semi-analytic solution, and (ii) convergence analysis of the radiated quadrupole waveforms for simulation d08q05 of Table I.

The geodesic slicing condition is enforced by setting the gauge functions to $\alpha = 1$, $\beta^i = 0$ throughout the evolution. The space part of the Reissner-Nordström solution in isotropic coordinates is given by Eq. (2.10) with a conformal factor [66,67]

$$\psi^2 = \left(1 + \frac{M}{2r}\right)^2 - \frac{Q^2}{4r^2}. \tag{5.1}$$

The time evolution of this solution is not known in closed analytic form, but the resulting metric components can be constructed straightforwardly via a simple integration procedure, cf. Appendix . As expected, we find a time evolution in this gauge to become numerically unstable at times τ of a few M. Before the breaking down of the evolution, however, we can safely compare the numerical and "analytical" solutions. This comparison is shown in Fig. 1 for the γ_{zz} component of the spatial metric and the E^z component of the electric field and demonstrates excellent agreement between the semianalytic and numerical results.

For the second test, we have evolved model d08q05 using three different resolutions as listed in Table I and extracted the gravitational and electromagnetic quadrupole ($l = 2$, $m = 0$) at $R_{\rm ex} = 100M$. For fourth-order convergence, we expect the differences between the higher resolution simulations to be a factor 2.78 smaller than their coarser resolution counterparts. The numerically obtained differences are displayed with the corresponding rescaling in Fig. 2. Throughout the physically relevant part of the waveform, we observe the expected fourth-order convergence. Only the spurious initial radiation (cf. the discussion at the end of Sec. III) at early times $\Delta t \lesssim -20$ in the figure exhibits convergence closer to second order, presumably a consequence of high-frequency noise contained in this spurious part of the signal. From Richardson extrapolation of our results we estimate the truncation error of the radiated waves to be about 1%. The error due to extraction at finite radius, on the other hand, is estimated to be 2% at $R_{\rm ex} = 100M$.

B. Collisions of two black holes: The "static" components and infall time

We start the discussion of our results with the behavior of the gravitational and electromagnetic multipoles when the system is in a nearly static configuration, i.e. shortly after the start of the simulation and at late stages after the ringdown of the postmerger hole. At these times, we expect our analytic predictions (4.3) and (4.4) for the monopole and dipole of the electromagnetic field to provide a rather accurate description. Furthermore, the total spacetime charge Q is conserved throughout the evolution, so that the monopole component of Φ_1 should be described by (4.3) *at all times*. The quadrupole, on the other hand, is expected to deviate significantly from the static prediction (4.4) when the black holes start moving fast.

As demonstrated in Fig. 3, we find our results to be consistent with this picture. Here we plot the monopole and quadrupole of Φ_1. The monopole part (left panel) captures the Coulomb field and can thus be compared with the total

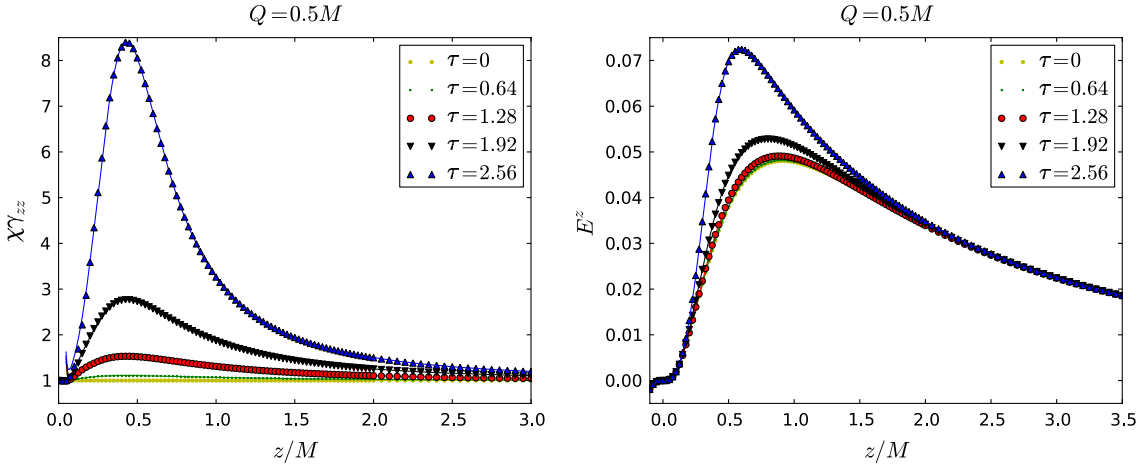

FIG. 1 (color online). The numerical profiles for γ_{zz} and E^z (symbols) obtained in geodesic slicing at various times τ are compared with the semianalytic results (lines).

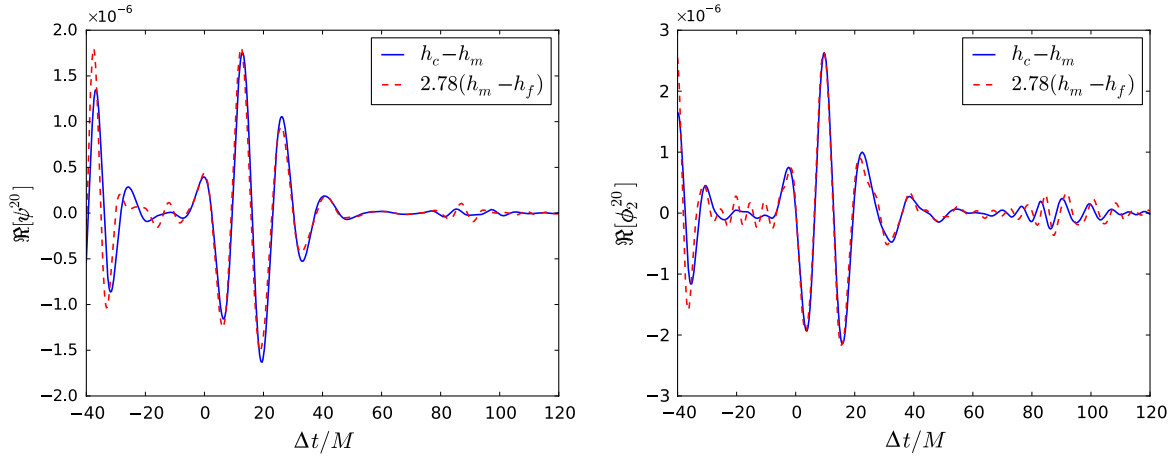

FIG. 2 (color online). Convergence analysis for simulation d08q05 of Table I with resolutions $h_c = M/64$, $h_m = M/80$, and $h_f = M/96$. The panels show differences of the (2, 0) multipoles of the real parts of Ψ_4 (left) and Φ_2 (right) extracted at $R_{\rm ex} = 100M$; in each case, the high-resolution differences have been rescaled by a factor of 2.78 as expected for fourth-order convergence.

charge of the system. It is constant throughout the evolution to within numerical error and shows agreement with the analytic prediction of Eq. (4.3) within numerical uncertainties; we measure a slightly smaller value for the monopole field than expected from the total charge of the system, but the measured value should increase with extraction radii and agree with the total charge expectation at infinity. This is consistent with the extrapolation of the measured value to infinity as shown in the figure. The quadrupole part (right panel) starts at a nonzero value in excellent agreement with Eq. (4.4), deviates substantially during the highly dynamic plunge and merger stage, and eventually rings down toward the static limit $\phi_1^{20} = 0$ as expected for a spherically symmetric charge distribution.

The analytic approximation of Sec. IV also predicts a value for the time of collision (4.9) for a given set of initial parameters. In particular, we see from this prediction that for fixed initial separation d and mass M the collision time scales with the charge as $t_{\rm collision} \sim 1/\sqrt{\mathcal{B}}$. In comparing these predictions with our numerical results we face the difficulty of not having an unambiguous definition of the separation of the black holes in the fully general relativistic case. From the entries in Table I we see that the proper distance L varies only mildly for fixed coordinate distance d up to $Q/M \approx 0.8$. For nearly extremal values of Q, however, L starts increasing significantly as expected from our discussion at the start of this section. We therefore expect the collision time of the numerical simulations rescaled by $\sqrt{\mathcal{B}}/t_0$, where t_0 is the corresponding time for the uncharged case, to be close to unity over a wide range of Q/M and show some deviation close to $Q/M = 1$. This expectation is borne out in Fig. 4 where we show this rescaled collision time, determined numerically as the first appearance of a common apparent horizon, as a function of Q/M.

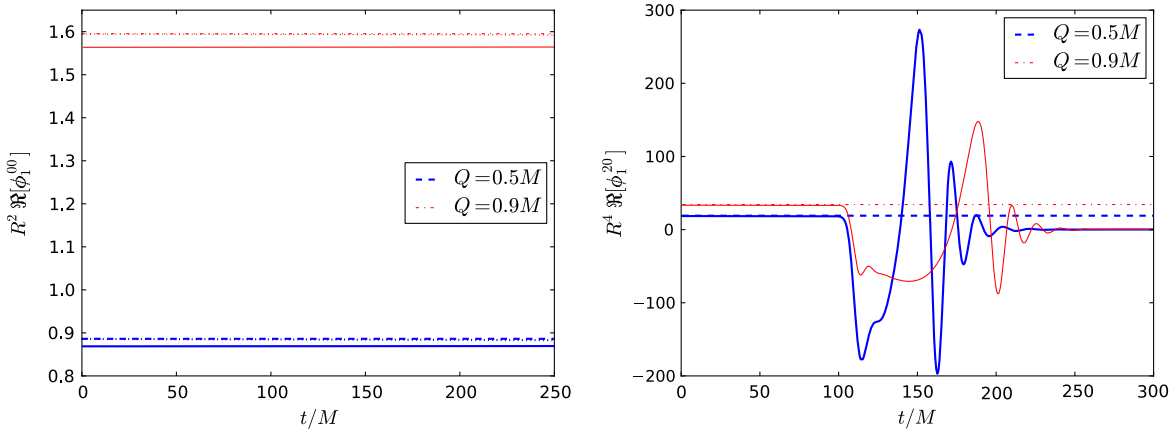

FIG. 3 (color online). Monopole ϕ_1^{00} (left) and quadrupole ϕ_1^{20} (right) of the radial part of the electromagnetic field Φ_1 extracted at $R_{\rm ex} = 100M$ for simulation d08q05 of Table I. The dashed curves show the predictions of Eqs. (4.3) and (4.4) at $R = \infty$ in the static limit. For the monopole case, we also added the curves obtained by extrapolating the results to infinite extraction radius; these curves—dotted lines—essentially overlap with the predictions from Eq. (4.3).

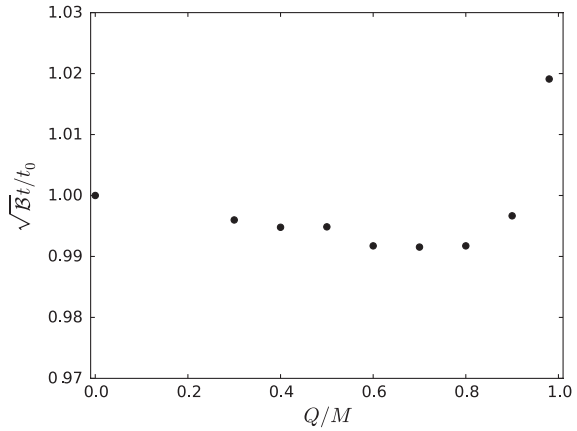

FIG. 4. Time for apparent horizon formation, rescaled by the factor $\sqrt{\mathcal{B}}$ and the apparent horizon formation time t_0 for an electrically neutral binary. We note that the change in the quantity we plot is only, at most, of 2%. The coordinate time itself, however, varies by a factor of 5 as one goes from $Q = 0$ to $Q = 0.98M$.

C. Waveforms: Infall, merger, and ringdown

The dynamical behavior of all our simulations is qualitatively well represented by the waveforms shown in Fig. 5 for simulations d16q00, d16q05 and d16q09. The panels show the real part of the gravitational (left) and electromagnetic (right) quadrupole extracted at $R_{\rm ex} = 100M$ as a function of time with $\Delta t = 0$ defined as the time of the global maximum of the waveform. From the classical analysis (4.10), we expect the waveforms Ψ_4, Φ_2 to scale roughly with $\mathcal{B}$ and the mass or charge of the black holes (the scaling with $\mathcal{B}$ is nontrivial, but both an analytic estimate and the numerical results indicate the scaling is approximately linear, which we shall therefore use for rescaling the plots in the figure).

The early stages of the signals are marked by the spurious radiation due to the construction of initial data, which we ignore in our analysis. Following a relatively weak phase of wave emission during the infall of the holes, the radiation increases strongly during the black-hole merger around $\Delta t = 0$ in Fig. 5 and decays exponentially as the final hole rings down into a stationary state. This overall structure of the signals is rather similar for the electromagnetic and the gravitational parts and follows the main pattern observed for gravitational-wave emission in head-on collisions of uncharged black holes [33,34].

The final, exponentially damped ringdown phase is well described by perturbation techniques [44]. In particular, charged black holes are expected to oscillate with two different types of modes, one of gravitational and one of electromagnetic origin. For the case of vanishing charge, the electromagnetic modes are not present, but they generally couple for charged black holes, and we expect both modes to be present in the spectra of our gravitational and electromagnetic waveforms. For verification we have fitted the late stages of the waveforms to a two-mode, exponentially damped sinusoid waveform

$$f(t) = A_1 e^{-i\omega_1 t} + A_2 e^{-i\omega_2 t}, \tag{5.2}$$

where A_i are real-valued amplitudes and ω_i complex frequencies. The results are summarized in Table II for selected values of the charge-to-mass ratio of the postmerger black hole. Real and imaginary parts of the fitted frequencies agree within a few percent or better with the perturbative predictions. For the large value Q/M, however, the wave signal is very weak and in such good agreement with a single ringdown mode (the gravitational one) that we cannot clearly identify a second, electromagnetic component. This feature is explained once we understand how the total radiated energy is distributed between the gravitational and the electromagnetic channels. For this purpose, we plot in Fig. 6 the Fourier spectrum of the relevant wave functions or, more precisely, their dominant quadrupole contributions obtained for simulation d08q03 $|\bar{\phi}^{20}|^2$, $|\bar{\psi}^{20}|^2$, where for any function f

$$\bar{f}(\omega) = \int_{-\infty}^{\infty} e^{i\omega t} f(t) dt. \tag{5.3}$$

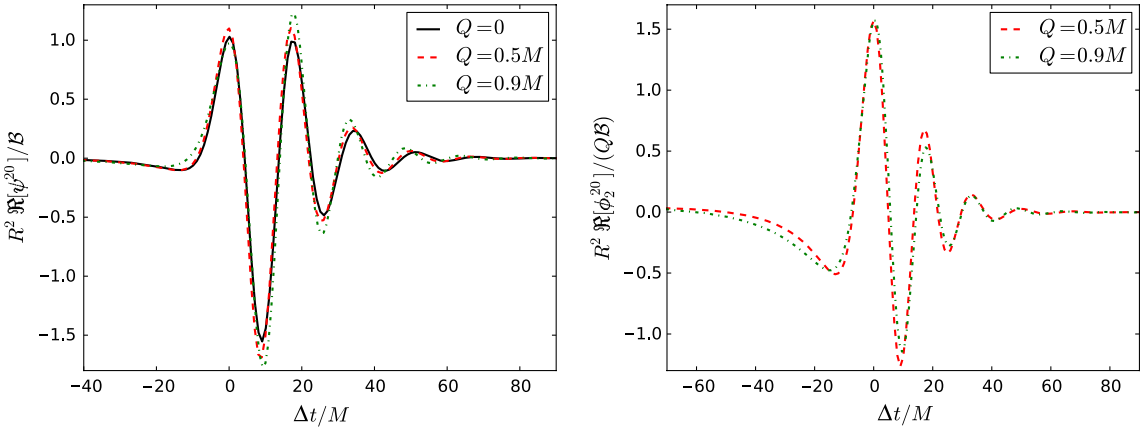

FIG. 5 (color online). Real part of the (2, 0) mode of Ψ_4 (left) and Φ_2 (right) extracted at $R_{\rm ex} = 100M$.

TABLE II. Comparison of the ringdown frequencies obtained from (i) perturbative calculations [44] and (ii) fitting a two-mode profile to the numerically extracted waveforms. For $Q/M = 0$ the electromagnetic modes are not excited. For values of $Q/M \geq 0.9$ the electromagnetic mode becomes so weak that we can no longer unambiguously identify it in the numerical data.

Q/M	$\omega_{1,2}^{\mathrm{QNM}}$	$\omega_{1,2}^{\mathrm{ext}}$
0	$0.374 - 0.0890i$	$0.374 - 0.088i$
	$0.458 - 0.0950i$	
0.3	$0.376 - 0.0892i$	$0.375 - 0.092i$
	$0.470 - 0.0958i$	$0.481 - 0.100i$
0.5	$0.382 - 0.0896i$	$0.381 - 0.091i$
	$0.494 - 0.0972i$	$0.511 - 0.096i$
0.9	$0.382 - 0.0896i$	$0.381 - 0.091i$
	$0.494 - 0.0972i$	?

It is clear from the figure that most of the energy is carried in the fundamental gravitational-wave-like mode with a peak at approximately $\omega \sim 0.37$, close to the oscillation frequency of the fundamental gravitational ringdown mode; see Table II.

D. Radiated energy and fluxes

The electromagnetic and gravitational-wave fluxes are given by Eqs. (3.9) and (3.10). We have already noticed from the waveforms in Fig. 5 that the electromagnetic signal follows a pattern quite similar to the gravitational one. The same holds for the energy flux that is shown in Fig. 7 for a subset of our simulations with $Q/M = 0$, 0.5, and 0.9. From the figure, as well as the numbers in Table I, we observe that the energy carried by gravitational radiation decreases with increasing Q/M, as the acceleration becomes smaller and quadrupole emission is suppressed, in agreement with prediction (4.14).

This is further illustrated in Fig. 8, which illustrates the radiated energy carried in the gravitational quadrupole and the electromagnetic quadrupole as well as their ratio as functions of the charge-to-mass ratio Q/M. For the case of vanishing charge, the total radiated energy is already known from the literature; e.g. [33]. The value increases mildly with the initial separation as a consequence of the slightly larger collision velocity but is generally found to be close to $E_{\mathrm{rad}}^{\mathrm{GW}}/M = 0.055\%$. Our values of 0.051% for $d/M \simeq 8$ and 0.055% for $d/M \simeq 16$ are in good agreement with the literature. As we increase Q/M, however, $E_{\mathrm{rad}}^{\mathrm{GW}}$ decreases significantly and for $Q/M = 0.9$ (0.98) has dropped by a factor of about 20 (10^3) relative to the uncharged case. For practical reasons, we have explored the largest ratio $Q/M = 0.98$ for the smaller initial separation $d/M \simeq 8$ only; the near cancellation of the gravitational and electromagnetic interaction and the resulting slowdown of the collision lead to a very long infall stage with essentially zero dynamics.

In contrast to the monotonically decreasing gravitational-wave energy, the electromagnetic signal reaches a local maximum around $Q/M = 0.6$, an expected observation as the electromagnetic radiation necessarily vanishes for $Q/M = 0$ (no charge) and $Q/M = 1$ (no acceleration) but takes on nonzero values in the regime in between. Closer analysis of our classical, flat-space calculation (4.13) predicts a maximum electromagnetic radiation output at

$$Q_{\max} = \sqrt{\frac{\sqrt{329} - 13}{14}} M \approx 0.605M, \tag{5.4}$$

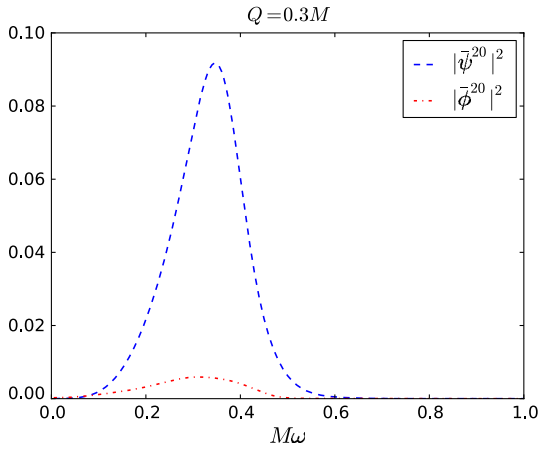

FIG. 6 (color online). Power spectrum for the gravitational (long dashed line) and electromagnetic (short dashed line) quadrupole extracted from simulation d08q03. Note that the spectrum peaks near the fundamental ringdown frequency of the gravitational mode; cf. Table II.

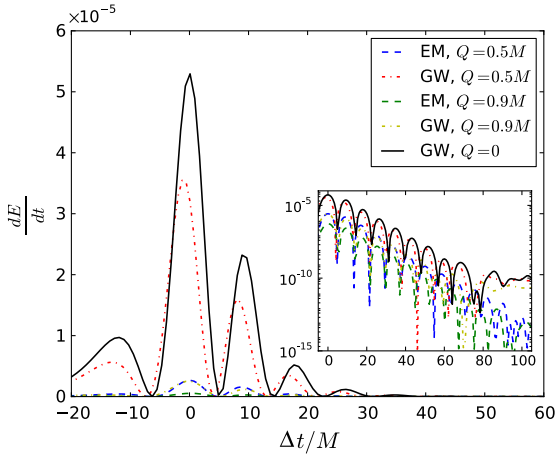

FIG. 7 (color online). Radiated fluxes for simulations d08q05, d08q09, and d08q00 of Table I. We have aligned the curves in time such that their global maximum coincides with $t = 0$. The inset shows the exact same plot with the y axis in logarithmic units.

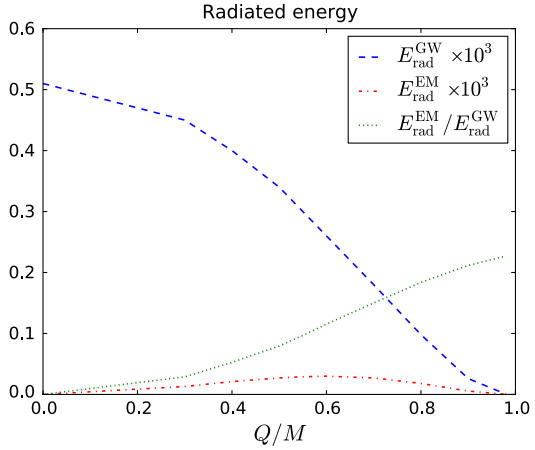

FIG. 8 (color online). Energy radiated in the gravitational and electromagnetic quadrupoles as well as the ratio of the two as a function of Q/M.

in excellent agreement with the results of our NR simulations.

We finally consider the ratio of electromagnetic to gravitational-wave energy (dotted curve in Fig. 8). As predicted by our analytic calculation (4.16), this ratio increases monotonically with Q/M for fixed separation d. A fit of our numerical results yields $E_{\rm rad}^{\rm EM}/E_{\rm rad}^{\rm GW} = 0.27Q^2/M^2$, and for our largest value $Q/M = 0.98$, we obtain a ratio of 0.227 to be compared with $\sim$0.24 as predicted by Eq. (4.16). Bearing in mind the simplicity of our analytic model in Sec. IV, the quantitative agreement is remarkable.

VI. FINAL REMARKS

We have performed a numerical study of collisions of charged black holes with equal mass and charge in the framework of the fully nonlinear Einstein-Maxwell equations. Our first observation is that the numerical relativity techniques (formulation of the evolution equations, gauge conditions, and initial data construction) developed for electrically neutral black-hole binaries can be straightforwardly extended to successfully model charged binaries even for nearly extremal charge-to-mass ratios $Q/M \lesssim 1$. In particular, we notice the contrast with the case of rotating black holes with nearly extremal spin, which represents a more delicate task for state-of-the-art numerical relativity; cf. Refs. [68,69] for the latest developments on this front. This absence of difficulties for charged holes is not entirely unexpected. Considering the construction of initial data, for instance, an important difference arises in the customary choice of conformally flat Bowen-York initial data [70], which greatly simplifies the initial data problem. While the Kerr solution for a single rotating black hole does not admit conformally flat slices [71] and therefore inevitably results in spurious radiation, especially for large spin parameters, this difficulty does not arise for charged but nonrotating black holes; cf. Equation (5.1) and Ref. [66].

The excellent agreement between the classical calculation for the energy emission and the numerical results reported here allow for an investigation of cosmic censorship close to extremality. If we take two black holes with $M_1 = M_2 = M/2$, $Q_1 = Q_2 = (M - \delta)/2$ and we let them fall from infinity, to first order in δ we get

$$Q_{\rm tot} = M - \delta, \qquad M_{\rm tot} = M - E_{\rm rad}. \tag{6.1}$$

Now, the classical result (4.14) implies that the dominant term for the radiated energy is $E_{\rm rad} \sim \mathcal{B}^{5/2}M \sim (\delta/M)^{5/2}M$. Thus we get

$$\frac{Q_{\rm tot}}{M_{\rm tot}} \simeq 1 - \frac{\delta}{M} + k\left(\frac{\delta}{M}\right)^{5/2}, \tag{6.3}$$

where k is a constant. We get the striking conclusion that cosmic censorship is preserved for charged collisions of nearly extremal holes ($\delta \ll M$), on account of the much longer collision time, which yields much lower velocities and therefore much lower energy output. The differences between the cases of spinning mergers and charged collisions are interesting. In the former case, naked singularities are avoided by radiation carrying away more angular momentum (via orbital hang-up [72]). In the latter case, our results suggest that naked singularities are avoided by the smaller radiation emission, due to the smaller accelerations involved in the infall.

It is even possible to construct binary initial data in closed analytic form, analogous to that of Brill-Lindquist data, for the special case of nonspinning binaries with equal charge-to-mass ratio starting from rest, and we have restricted our present study to this case. Specifically, we have evolved a sequence of binaries with Q/M varying from zero to values close to extremality. Starting with the electrically neutral case, where our gravitational-wave emission $E_{\rm rad}^{\rm GW}/M = 0.055\%$ agrees well with the literature, we observe a monotonic decrease of the emitted gravitational-wave energy as we increase Q/M. For our largest value $Q/M = 0.98$, $E_{\rm rad}^{\rm GW}$ is reduced by about 3 orders of magnitude, as the near cancellation of the gravitational and electromagnetic forces substantially slows down the collision. In contrast, the radiated electromagnetic energy reaches a maximum near $Q/M = 0.6$ but always remains significantly below its gravitational counterpart. Indeed, the ratio $E_{\rm rad}^{\rm EM}/E_{\rm rad}^{\rm GW}$ increases monotonically with Q/M and approaches about 25% in the limit $Q/M \to 1$. We find all these results to be in remarkably good qualitative *and* quantitative agreement with analytic approximations obtained in the framework of the dynamics of two point charges in a Minkowski background. This approximation also predicts that the collision time relative to that of the uncharged case scales $\sim\sqrt{1 - Q^2/M^2}$, which is confirmed within a few percent by our numerical simulations.

Our present study paves the way for various future extensions. Quite naturally, it will be important to consider more generic types of initial data in order to tackle some of the issues discussed in the Introduction. A nonzero boost, for instance, will allow us to study both binary black-hole systems that will coalesce into a Kerr-Newman black hole and the impact of electric charge on the dynamics of and wave emission (electromagnetic and gravitational) in high-energy collisions. In this context the robustness of our simulations is particularly encouraging, as we have not encountered stability issues as observed in the study of black-hole collisions in higher-dimensional spacetimes [73].

A further interesting extension presently under study is the case of oppositely charged black holes. Quite likely, the remarkable accuracy of our simple analytic models is in part due to the relatively small, ''nonrelativistic'' collision speeds caused by the electric repulsion of the equal charges. Furthermore, the gravitational quadrupole formula (4.14) will still apply for opposite charges, but then $\mathcal{B} = 1 + Q^2/M^2$, and the formula predicts an enhancement of almost 2 orders of magnitude in the gravitational radiation emitted when going from $Q = 0$ to $Q = M$ (without accounting for additional contributions due to dipole radiation and to Bremsstrahlung by accelerated charges). This would release about 3% of the total center of mass energy as gravitational waves. Even more impressive is the possibility of observing a huge splash of electromagnetic energy when both holes are nearly extremal. The area theorem, which yields a poor estimate in the neutral case, bounds the total radiation to be less than $\sim$65% the CM energy; how close one gets to this number is up to nonlinear evolutions of the kind reported in this work.

ACKNOWLEDGMENTS

We are indebted to Leonardo Gualtieri, Steve Giddings, and Emanuele Berti for fruitful discussions on this topic. We further thank the anonymous referee for suggesting the calculation of the charge-to-mass ratio of the merged hole, in particular, in the near extremal limit. M. Z. would like to thank the Perimeter Institute for Theoretical Physics for its hospitality, through the Visiting Graduate Fellows program, where this work was done. The authors thank the Yukawa Institute for Theoretical Physics at Kyoto University, where parts of this work were completed during the YITP-T-11-08 on ''Recent advances in numerical and analytical methods for black hole dynamics.'' M. Z. is funded by FCT through Grant No. SFRH/BD/43558/2008. U. S. acknowledges support from the Ramón y Cajal Programme and Grant No. FIS2011-30145-C03-03 of the Ministry of Education and Science of Spain, the NSF TeraGrid and XSEDE Grant No. PHY-090003, RES Grants No. AECT-2012-1-0008 and No. AECT-2011-3-0007 through the Barcelona Supercomputing Center, and CESGA Grants No. ICTS-200 and No. ICTS-221. This work was supported by the *DyBHo–256667* ERC Starting Grant, the *CBHEO–293412* FP7-PEOPLE-2011-CIG Grant, the *NRHEP–295189* FP7-PEOPLE-2011-IRSES Grant, and by FCT–Portugal through Projects No. PTDC/FIS/098025/2008, No. PTDC/FIS/098032/2008, No. PTDC/FIS/116625/2010, and No. CERN/FP/116341/2010, the Sherman Fairchild Foundation to Caltech, as well as NSERC through a Discover Grant and CIFAR. Research at Perimeter Institute is supported through Industry Canada and by the Province of Ontario through the Ministry of Research & Innovation. Computations were performed on the Blafis Cluster at Aveiro University, the Milipeia in Coimbra, the Lage Cluster at Centro de Física do Porto, the Bifi Cluster of the University of Zaragoza, the CESGA Cluster Finis Terrae, NICS Kraken, and the SDSC Cluster Trestles.

APPENDIX A: GEODESIC SLICING

In the usual Schwarzschild-like coordinates, the Reissner-Nordström line element and electromagnetic potential are given by

$$ds^2 = -f(R)dt^2 + \frac{dR^2}{f(R)} + R^2 d\Omega_2,$$
$$A = -\frac{Q}{R}dt, \tag{A1}$$

where $f(R) = 1 - \frac{2M}{R} + \frac{Q^2}{R^2}$. For a radially infalling massive particle, starting from rest at $R = R_0$, the energy per unit mass is $\sqrt{f(R_0)}$. The geodesic equation (for infalling particles) may then be written as

$$\frac{dt}{d\tau} = \frac{\sqrt{f(R_0)}}{f(R)}, \qquad \frac{dR}{d\tau} = -\sqrt{f(R_0) - f(R)}. \tag{A2}$$

With these equations and the initial condition $R(\tau = 0) = R_0$, we can numerically integrate this system and thus have $R = R(\tau, R_0)$. Assuming such a coordinate transformation, $(t, R) \rightarrow (\tau, R_0)$, the metric takes the form

$$ds^2 = -d\tau^2 + \left(\frac{\partial R(\tau, R_0)}{\partial R_0}\right)^2 \frac{dR_0^2}{f(R_0)} + R(\tau, R_0)^2 d\Omega_2. \tag{A3}$$

It remains now to perform the coordinate transformation $R_0 \rightarrow r$ that guarantees the metric an isotropic form at $\tau = 0$. This can be accomplished with

$$\frac{dr}{r} = \frac{dR_0}{R_0\sqrt{f(R_0)}}; \tag{A4}$$

integrating we obtain

$$R_0(r) = r\left[\left(1 + \frac{M}{2r}\right)^2 - \frac{Q^2}{4r^2}\right]. \tag{A5}$$

The final form for the metric is then

$$ds^2 = -d\tau^2 + \left(\frac{R_0(r)}{r}\right)^2\left[\left(\frac{\partial R(\tau, R_0)}{\partial R_0}\right)^2 dr^2 + \left(\frac{r}{R_0(r)}\right)^2 R(\tau, R_0(r))^2 d\Omega_2\right]. \quad \text{(A6)}$$

Since, by assumption, $R(\tau = 0) = R_0$, $\frac{\partial R}{\partial R_0}|_{\tau=0} = 1$, this metric is indeed in isotropic form at $\tau = 0$.

[1] F. Pretorius, Phys. Rev. Lett. **95**, 121101 (2005).
[2] J. G. Baker, J. Centrella, D.-I. Choi, M. Koppitz, and J. van Meter, Phys. Rev. Lett. **96**, 111102 (2006).
[3] M. Campanelli, C. O. Lousto, P. Marronetti, and Y. Zlochower, Phys. Rev. Lett. **96**, 111101 (2006).
[4] F. Pretorius, arXiv:0710.1338.
[5] C. Palenzuela, M. Anderson, L. Lehner, S. L. Liebling, and D. Neilsen, Phys. Rev. Lett. **103**, 081101 (2009).
[6] C. Palenzuela, L. Lehner, and S. L. Liebling, Science **329**, 927 (2010).
[7] J. Centrella, J. G. Baker, B. J. Kelly, and J. R. van Meter, Rev. Mod. Phys. **82**, 3069 (2010).
[8] M. Campanelli, C. O. Lousto, B. C. Mundim, H. Nakano, Y. Zlochower, and H.-P. Bischof, Classical Quantum Gravity **27**, 084034 (2010).
[9] U. Sperhake, E. Berti, and V. Cardoso, arXiv:1107.2819.
[10] H. P. Pfeiffer, arXiv:1203.5166.
[11] T. Baumgarte, P. R. Brady, J. D. E. Creighton, L. Lehner, F. Pretorius, and R. DeVoe, Phys. Rev. D **77**, 084009 (2008).
[12] B. Aylott *et al.*, Classical Quantum Gravity **26**, 114008 (2009).
[13] J. Abadie *et al.* (The LIGO Scientific Collaboration and the Virgo Collaboration), Phys. Rev. D **83**, 122005 (2011).
[14] P. Ajith *et al.*, arXiv:1201.5319.
[15] J. Abadie *et al.* (The LIGO Scientific Collaboration and the Virgo Collaboration), arXiv:1201.5999.
[16] G. Gibbons, Commun. Math. Phys. **44**, 245 (1975).
[17] R. Blandford and R. Znajek, Mon. Not. R. Astron. Soc. **179**, 433 (1977).
[18] J. Hartle and S. Hawking, Commun. Math. Phys. **26**, 87 (1972).
[19] S. Majumdar, Phys. Rev. **72**, 390 (1947).
[20] A. Papapetrou, Proc. R. Irish Acad., Sect. A **52**, 11 (1948).
[21] G. Gibbons and C. Hull, Phys. Lett. **109B**, 190 (1982).
[22] K. Tod, Phys. Lett. **121B**, 241 (1983).
[23] N. Manton, Phys. Lett. **110B**, 54 (1982).
[24] R. C. Ferrell and D. M. Eardley, Phys. Rev. Lett. **59**, 1617 (1987).
[25] G. 't Hooft, Phys. Lett. B **198**, 61 (1987).
[26] M. W. Choptuik and F. Pretorius, Phys. Rev. Lett. **104**, 111101 (2010).
[27] H. Yoshino and R. B. Mann, Phys. Rev. D **74**, 044003 (2006).
[28] D. M. Gingrich, J. High Energy Phys. 02 (2007) 098.
[29] U. Sperhake, V. Cardoso, F. Pretorius, E. Berti, and J. A. Gonzalez, Phys. Rev. Lett. **101**, 161101 (2008).
[30] M. Shibata, H. Okawa, and T. Yamamoto, Phys. Rev. D **78**, 101501 (2008).
[31] U. Sperhake *et al.*, Phys. Rev. Lett. **103**, 131102 (2009).
[32] M. Zilhao *et al.*, Phys. Rev. D **81**, 084052 (2010).
[33] H. Witek, M. Zilhao, L. Gualtieri, V. Cardoso, C. Herdeiro A. Nerozzi, and U. Sperhake, Phys. Rev. D **82**, 104014 (2010).
[34] H. Witek, V. Cardoso, L. Gualtieri, C. Herdeiro, U. Sperhake, and M. Zilhao, Phys. Rev. D **83**, 044017 (2011).
[35] H. Okawa, K.-i. Nakao, and M. Shibata, Phys. Rev. D **83**, 121501 (2011).
[36] P. M. Chesler and L. G. Yaffe, Phys. Rev. Lett. **102**, 211601 (2009).
[37] M. Shibata and H. Yoshino, Phys. Rev. D **81**, 021501 (2010).
[38] L. Lehner and F. Pretorius, Phys. Rev. Lett. **105**, 101102 (2010).
[39] H. M. S. Yoshino and M. Shibata, Prog. Theor. Phys. Suppl. **189**, 269 (2011).
[40] V. Cardoso *et al.*, arXiv:1201.5118.
[41] R. M. Wald, Phys. Rev. D **10**, 1680 (1974).
[42] C. Palenzuela, T. Garrett, L. Lehner, and S. L. Liebling, Phys. Rev. D **82**, 044045 (2010).
[43] S. Chandrasekhar, *The Mathematical Theory of Black Holes* (Oxford University Press, New York, 1983).
[44] E. Berti, V. Cardoso, and A. O. Starinets, Classical Quantum Gravity **26**, 163001 (2009).
[45] L. Blanchet, Living Rev. Relativity **9**, 4 (2006), http://www.livingreviews.org/lrr-2006-4.
[46] M. Boyle, D. A. Brown, L. E. Kidder, A. H. Mroue, H. P. Pfeiffer, M. A. Scheel, G. B. Cook, and S. A. Teukolsky, Phys. Rev. D **76**, 124038 (2007).
[47] U. Sperhake, B. Brügmann, D. Müller, and C. F. Sopuerta, Classical Quantum Gravity **28**, 134004 (2011).
[48] C. Palenzuela, L. Lehner, O. Reula, and L. Rezzolla, Mon. Not. R. Astron. Soc. **394**, 1727 (2009).
[49] C. Palenzuela, L. Lehner, and S. Yoshida, Phys. Rev. D **81**, 084007 (2010).
[50] P. Mosta, C. Palenzuela, L. Rezzolla, L. Lehner, S. Yoshida, and D. Pollney, Phys. Rev. D **81**, 064017 (2010).
[51] D. R. Brill and R. W. Lindquist, Phys. Rev. **131**, 471 (1963).
[52] M. Alcubierre, J. C. Degollado, and M. Salgado, Phys. Rev. D **80**, 104022 (2009).
[53] S. Komissarov, arXiv:0708.0323.
[54] M. Alcubierre, *Introduction to* 3 + 1 *Numerical Relativity*, International Series of Monographs on Physics (Oxford University Press, Oxford, 2008).
[55] E. Gourgoulhon, arXiv:gr-qc/0703035.
[56] M. Alcubierre, B. Bruegmann, P. Diener, M. Koppitz, D. Pollney, E. Seidel, and R. Takahashi, Phys. Rev. D **67**, 084023 (2003).
[57] U. Sperhake, Phys. Rev. D **76**, 104015 (2007).
[58] L. Lehner and O. M. Moreschi, Phys. Rev. D **76**, 124040 (2007).

[59] E. T. Newman and R. Penrose, J. Math. Phys. (N.Y.) **3**, 566 (1962).
[60] J. D. Jackson, *Classical Electrodynamics* (Wiley, New York, 1998), 3rd ed.
[61] Cactus Computational Toolkit, http://www.cactuscode.org/.
[62] E. Schnetter, S. H. Hawley, and I. Hawke, Classical Quantum Gravity **21**, 1465 (2004).
[63] Mesh refinement with Carpet, http://www.carpetcode.org/.
[64] J. Thornburg, Classical Quantum Gravity **21**, 743 (2004).
[65] J. Thornburg, Phys. Rev. D **54**, 4899 (1996).
[66] J. C. Graves and D. R. Brill, Phys. Rev. **120**, 1507 (1960).
[67] B. Reimann and B. Bruegmann, Phys. Rev. D **69**, 044006 (2004).
[68] G. Lovelace, M. Boyle, M. A. Scheel, and B. Szilagyi, Classical Quantum Gravity **29**, 045003 (2012).
[69] C. O. Lousto, H. Nakano, Y. Zlochower, B. C. Mundim, and M. Campanelli, Phys. Rev. D **85**, 124013 (2012).
[70] J. M. Bowen and J. W. York, Jr., Phys. Rev. D **21**, 2047 (1980).
[71] A. Garat and R. H. Price, Phys. Rev. D **61**, 124011 (2000).
[72] M. Campanelli, C. Lousto, and Y. Zlochower, Phys. Rev. D **74**, 041501 (2006).
[73] M. Zilhao, M. Ansorg, V. Cardoso, L. Gualtieri, C. Herdeiro, U. Sperhake, and H. Witek, Phys. Rev. D **84**, 084039 (2011).